Geochemistry Geophysics Geosystems G3
AN ELECTRONIC JOURNAL OF THE EARTH SCIENCES
Published by AGU and the Geochemical Society

Article
Volume 9, Number 6
21 June 2008
Q06008, doi:10.1029/2008GC001952
ISSN: 1525-2027

Magnetic study of mafic granulite xenoliths from the Hannuoba basalt, north China

Qingsheng Liu
Department of Geophysics, China University of Geosciences, Wuhan 430074, China (lqs321@cug.edu.cn)

Qingsong Liu
Paleomagnetism and Geochronology Laboratory (SKL-LE), Institute of Geology and Geophysics, Chinese Academy of Sciences, Beijing 100029, China

Yongsheng Liu
State Key Laboratory of Geological Processes and Mineral Resources of China, China University of Geosciences, Wuhan 430074, China

Shan Gao
State Key Laboratory of Geological Processes and Mineral Resources of China, China University of Geosciences, Wuhan 430074, China

State Key Laboratory of Continental Dynamics, Northwest University, Xi'an 710069, China

Tao Yang and Yinhe Luo
Department of Geophysics, China University of Geosciences, Wuhan 430074, China

Zhenmin Jin
State Key Laboratory of Geological Processes and Mineral Resources of China, China University of Geosciences, Wuhan 430074, China

[1] The composition and structure of the lower continental crust are of great interest in understanding the dynamic processes of the Earth interior. In this study, we examined relationships between the magnetic properties and opaque mineralogy of a set of mafic granulite xenoliths (derived from ~24–41 km) collected from the Hannuoba region, north China (a region well known for its exposures of lower crustal rocks). These mafic granulite xenoliths are weakly magnetic with an average magnetic susceptibility (χ, mass specific) and saturation isothermal remanent magnetization (SIRM) of 5.87×10^{-7} m^3 kg^{-1} and 31.53×10^{-4} Am^2 kg^{-1}, respectively. The opaque minerals identified by electron microprobe (EMP) analysis in mafic granulite xenoliths are mainly paramagnetic Mg-rich ilmenite, which significantly contributed the room temperature χ. In contrast, SIRM are controlled predominately by pyrrhotite and magnetite, which were clearly identified by both scanning electron microscopy (SEM) and rock magnetic analyses. Our results show some relationships between these magnetic properties and the ratio of concentrations of the trace rare earth elements (La/Yb), which is sensitive to degree of fractional crystallization. More significantly, the Mg content in ilmenite is highly related to the fractional crystallization. These observations bring new insights into the complexities of the magnetic properties and the mineral composition (e.g., ilmenite) during the dynamic processes of mafic granulite xenoliths formation. However, the exact relationship between the rock magnetism and the fractional crystallization process needs further studies.

Components: 7013 words, 10 figures, 4 tables.

Keywords: mafic granulite xenolith; rock magnetism; opaque mineralogy; fractional crystallization; Hannuoba; north China.

Index Terms: 1540 Geomagnetism and Paleomagnetism: Rock and mineral magnetism; 1519 Geomagnetism and Paleomagnetism: Magnetic mineralogy and petrology; 3660 Mineralogy and Petrology: Metamorphic petrology.

Received 19 January 2008; **Revised** 29 April 2008; **Accepted** 6 May 2008; **Published** 21 June 2008.

Liu, Q., Q. Liu, Y. Liu, S. Gao, T. Yang, Y. Luo, and Z. Jin (2008), Magnetic study of mafic granulite xenoliths from the Hannuoba basalt, north China, *Geochem. Geophys. Geosyst.*, *9*, Q06008, doi:10.1029/2008GC001952.

1. Introduction

[2] The composition and structure of the lower continental crust are crucial for understanding crustal formation and evolution, and crust-mantle interaction [*Kay and Kay*, 1981; *Rudnick and Fountain*, 1995]. Long-wavelength magnetic anomalies are generally considered to originate from the deep crust [*Wasilewski and Mayhew*, 1982; *Arkani-Hamed and Strangway*, 1985; *Arkani-Hamed and Dyment*, 1996; *Pikington and Percival*, 1999, 2001; *Q. S. Liu et al.*, 2004; *Hemant and Maus*, 2005]. Although the chemical composition of the lower continental crust is well constrained [*Rudnick*, 1992; *Rudnick and Fountain*, 1995; *Rudnick and Gao*, 2003], some of its physical properties (e.g., rock magnetism) are still controversial.

[3] The lower continental crust, which is composed of granulite-facies metamorphic rocks, is generally accessible either as large tracts of surface outcrops (terrains) or as tiny fragments carried from greater depths in volcanic conduits (xenoliths) [*Rudnick*, 1992; *Shive et al.*, 1992; *Downes*, 1993]. Granulite-facies metamorphism would significantly change the petrophysical properties (e.g., density, magnetism, seismic velocity and rheology) in response to the geodynamic process of the lower crust and this would affect the geophysical imaging.

[4] Previous magnetic studies have focused mostly on the exposed crustal rocks, e.g., deep crustal section at Ivrea zone, Italy [*Wasilewski and Fountain*, 1982; *Wasilewski and Warner*, 1988; *Belluso et al.*, 1990], the Lofoten-Vesteralen terrain of Norway [*Schlinger*, 1985; *Schlinger and Veblen*, 1989], the Pikwitonei-Cross lake subprovinces in Central Manitoba [*Willams et al.*, 1985], the Kapuskasing uplift of Ontario, Canada [*Shive and Fountain*, 1988], the granulite-terrane around Wilson Lake, Labrador, Canada [*Kletetschka and Wasilewski*, 2002], metamorphic rock from the Russell Belt, northern Adirondack Mountains, New York [*Kasama et al.*, 2004] and Dengfeng-Lushan section, south margin of North China Craton and Wutai-Jining crust section of North China Craton [*Liu and Gao*, 1992; *Liu et al.*, 2000], Arunta block of central Australia [*Kelso et al.*, 1993] and the Sulu UHP belt, eastern China [*Liu et al.*, 2007]. Studies on the magnetic properties of xenoliths from much deeper crust and even the upper mantle remain scarce [*Wasilewski*, 1987; *Liu and Lu*, 1992; *Warner and Wasilewski*, 1995, 1997].

[5] Rock magnetic properties are known to be controlled by: amount and type of magnetic mineralogy, modifications of the mineralogy by metamorphism, and imparted anisotropy if any [*Haggerty and Toft*, 1985; *Shive and Fountain*, 1988; *Schlinger and Veblen*, 1989; *Ramachandran*, 1990; *Zhang and Piper*, 1994; *Kletetschka and Wasilewski*, 2002; *Pechersky and Genshaft*, 2002; *McEnroe et al.*, 2004]. The microstructural mechanisms dominating the magnetic signatures of the magnetic minerals in the lower crust is presently unclear, although exsolution lamellae in the hematite-ilmenite series has been proposed as one possible source of the magnetism in deep crust [*McEnroe et al.*, 2001; *Robinson et al.*, 2002, 2004; *Kasama et al.*, 2004].

[6] In this study, we investigate magnetic, geochemical and mineralogical properties of the mafic granulite xenoliths from the Hannuoba basalt, north China (Figure 1). Previous geochemical and geochronology studies have been conducted by *Liu et al.* [2001] and *Y. S. Liu et al.* [2004]. Thus these samples provide a unique opportunity to examine

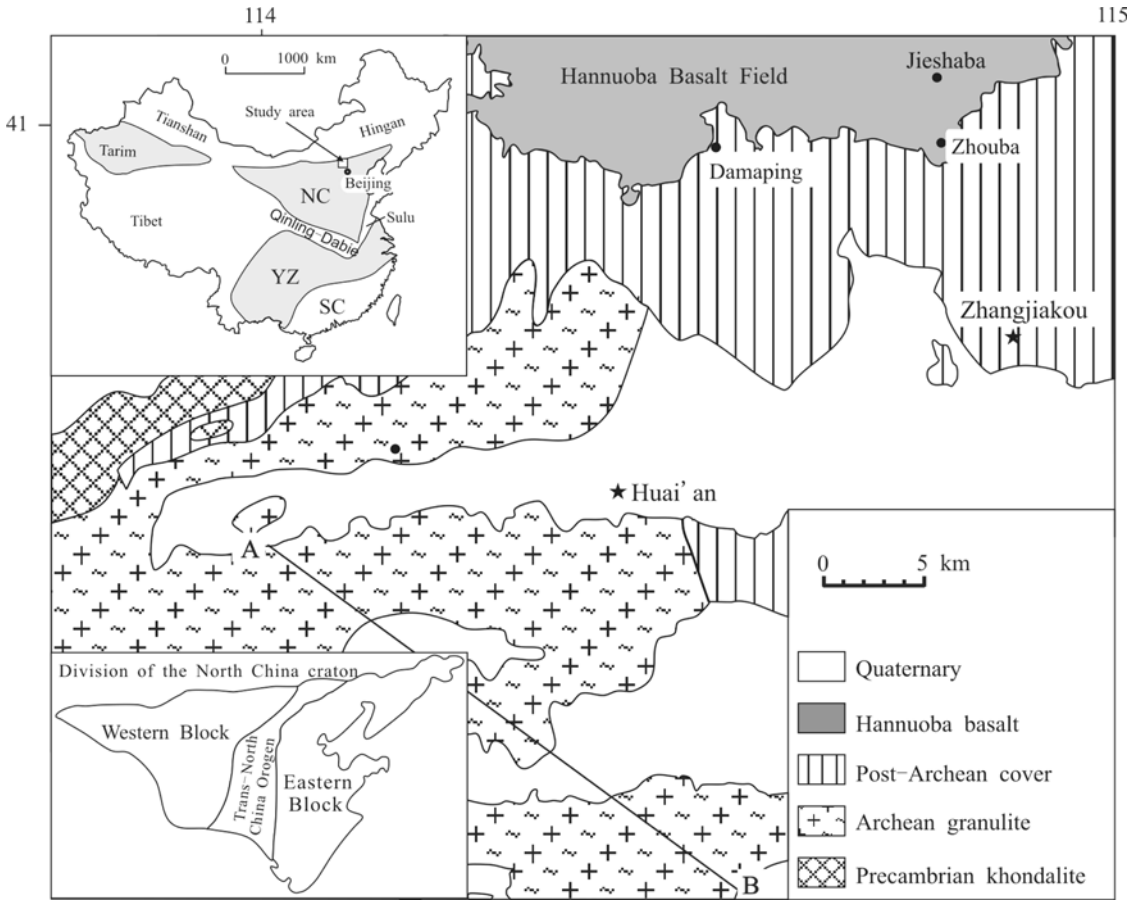

Figure 1. Simplified geological map of the Hannuoba area. Inset shows the location of the study area and tectonic division of China. NC, North China Craton; YC, Yangtze Craton; SC, South China Orogen. The division of the North China Craton is after *Zhao et al.* [2000].

the relationships between rock magnetism, opaque mineralogy and fractional crystallization.

2. Geological Settings

[7] On the basis of the age, lithological assemblage, tectonic evolution and P-T-t paths, the North China Craton can be divided into three parts: the Eastern Block, the Western Block and the intervening Trans-North China Orogen/Central Orogenic Belt (Figure 1). The North China Craton has experienced widespread tectonothermal reactivation during the Late Mesozoic and Cenozoic, as indicated by emplacement of voluminous Late Mesozoic granites and extensive Tertiary volcanism of alkaline basalt carrying abundant mantle xenoliths [*Zhao et al.*, 2000].

[8] The Hannuoba basalts occur along the northern margin of the Trans-North China Orogen (Figure 1), covering an area of > 1700 km^2. The basalts are dated at ~14–27 Ma by the K-Ar method [*Zhu*, 1998]. Lower crustal and upper mantle xenoliths carried by alkaline basalts show diverse lithologies. Mantle peridotite xenoliths are dominated by spinel lherzolites with minor websterites. Granulite xenoliths are dominantly mafic and intermediate with rare metasedimentary members. Previously estimated P-T data suggests equilibrium temperatures of 900–1000°C and 0.9–1.5 GPa for mafic granulites [*Chen et al.*, 2001; *Liu et al.*, 2001, 2003]. By referring to the Nushan geotherm, the combination of estimated temperature and the calculated V_p suggests that the mafic granulites derived from ~32–41 km [*Liu et al.*, 2001]. Zircon dating indicates that the mafic granulites formed during the Mesozoic (~120–140 Ma) [*Fan et al.*, 1998; *Liu et al.*, 2001; *Y. S. Liu et al.*, 2004; *Wilde et al.*, 2003], and include old zircons with an upper intercept age of ~2.5 Ga present in a few intermediate granulites [*Y. S. Liu et al.*, 2004].

Table 1. Mineral Assemblages and Petrographic Descriptions of the Studied Samples[a]

Sample	Mineral Assemblage	Petrographic Descriptions
DMP03	Cpx + Pl + Opx + An	Medium equigranular plagioclase, orthopyroxene and clinopyroxene with minor anorthoclase. Layering is defined by relative concentrations of plagioclase and pyroxene.
DMP09	Cpx + Opx + Pl + An	Coarse and equigranular clinopyroxene, orthopyroxene and plagioclase with minor anorthoclase. Layering is defined by relative concentrations of plagioclase and pyroxene.
DMP28	Cpx + Pl + Opx + An	Coarse and equigranular clinopyroxene, plagioclase and orthopyroxene with minor anorthoclase.
DMP45	Cpx + Pl + Opx + An + Ru + Opq	Medium- to coarse-grained clinopyroxene, plagioclase, orthopyroxene, with minor rutile, anorthoclase and opaque minerals. Layering is defined by relative concentrations of plagioclase and pyroxene.
DMP66	Cpx + Opx + Pl + An	Coarse and equigranular clinopyroxene, orthopyroxene, plagioclase with minor anorthoclase. Subtle layering is defined by concentrations and preferred orientations of plagioclase and pyroxene.
DMP68	Cpx + Opx + Pl + Scap + An + Opq	Coarse-equigranular polygonal clinopyroxene, orthopyroxene and plagioclase with minor anorthoclase and opaque minerals. Thick layering (>1 cm) is defined by plagioclase-rich and pyroxene-rich layers.
DMP71	Cpx + Opx + Pl + An	Medium equigranular clinopyroxene, plagioclase, orthopyroxene with minor anorthoclase.
DMP72	Cpx + Opx + Pl + An + Ru	Medium- to coarse-grained clinopyroxene, plagioclase, orthopyroxene, with minor rutile and anorthoclase. Plagioclase contains abundant exsolution lamellae of feldspar. Foliation moderately developed by preferred orientation of pyroxene and plagioclase.

[a] Pl, plagioclase; An, anorthoclase; Cpx, clinopyroxene; Opx, orthopyroxene; Opq, opaque mineral; Ru, rutile; Scap, scapolite.

[9] The mineralogy and geochemistry of the mafic granulite xenoliths (Table 1) clearly indicates an igneous origin [*Liu et al.*, 2001; *Y. S. Liu et al.*, 2004]. For example, *Liu et al.* [2001] documented continuous thick layers (~1 cm) of alternating plagioclase and pyroxene in samples DMP-68 and DMP-70, which points to their origin as products of accumulation in a magma chamber. Convex REE patterns with a maximum at Nd and positive Eu anomalies for mafic granulites are typical of plagioclase-clinopyroxene-rich cumulates derived from LREE-enriched magmas [*Liu et al.*, 2001]. This is also supported by the positive correlations between Cr, Ni and $Mg^{\#}$ of these xenoliths. The Ni-Cr and La-Yb variations and positive Eu anomalies of these xenoliths can be well modeled by fractional crystallization of pyroxene + olivine and/or pyroxene + plagioclase [*Liu et al.*, 2001], which agrees with the occurrence of igneous zircons with ages of 97–158 Ma found in olivine-bearing pyroxenites [*Y. S. Liu et al.*, 2004]. All these observations suggest that the mafic granulite xenoliths were products of ~160–140 Ma basaltic underplating and ~140–80 Ma granulite-facies metamorphism [*Y. S. Liu et al.*, 2004].

3. Samples and Experiments

[10] The studied xenoliths range from 4 to 20 cm in diameter. To minimize the effects of invasion of host basalt or possible surface weathering, the margins of the xenoliths were sawed off. The fresh inner parts were used for making thin sections. Fresh samples were also crushed to ~60 meshes in a steel-jaw crusher for geochemical analysis [*Liu et al.*, 2001].

[11] Major element analyses of the whole rock samples were conducted by X-ray fluorescence (XRF). Trace elements were analyzed using an Elan 6000 inductively coupled plasma mass spectrometer (ICP-MS). The sample preparation procedures were summarized by *Liu et al.* [2001]. The

Table 2. The χ, SIRM, and Geochemical Compositions of the Hannuoba Xenoliths[a]

Number	χ (10^{-7} m^3 kg^{-1})	SIRM (10^{-4}Am^2 kg^{-1})	SiO_2	TiO_2	Al_2O_3	Fe_2O_3	FeO	MgO	CaO	MnO	Na_2O	K_2O	P_2O_5	H_2O+	CO_2	La	Yb	Sr	Co	V	Mg#
3	2.55	4.81	49.07	0.48	13.84	0.83	5.97	14.01	10.99	0.12	1.26	0.51	0.03	2.47	0.03	6.74	1.06	682	47.26	116	78.9
9	4.65	5.93	49.54	0.49	9.65	1.17	8.33	18.37	8.17	0.15	1.23	0.35	0.02	2.11	0.03	3.59	0.88	595	59.94	134	77.9
28	6.40	85.49	50.30	0.64	9.57	1.76	9.02	13.85	11.42	0.18	1.35	0.38	0.04	1.15	0.04	3.23	0.96	462	64.45	203	70.2
45	6.90	30.23	50.66	0.36	11.61	1.23	8.25	15.06	8.62	0.16	1.51	0.49	0.02	1.71	0.03	1.96	0.54	714	58.46	133	74.3
66	4.71	15.16	50.51	0.42	12.1	0.94	6.17	13.58	12.14	0.12	1.62	0.33	0.02	1.71	0.03	2.98	0.61	674	47.81	140	77.7
68	5.60	48.14	49.74	0.41	9.41	0.74	7.75	16.23	11.30	0.15	1.91	0.17	0.03	1.81	0.07	2.48	0.57	479	59.16	149	77.6
71	9.33	38.97	49.60	0.60	9.61	1.58	8.57	13.98	12.12	0.17	1.21	0.47	0.05	1.63	0.09	3.79	0.89	460	58.26	189	71.6
72	6.81	23.93	49.70	0.73	7.07	1.80	11.25	18.41	8.12	0.20	0.79	0.32	0.04	1.26	0.03	4.59	1.53	254	70.98	159	72.6

[a] Here, χ is mass susceptibility; SIRM is saturation isothermal remanent magnetization. Major oxides are reported in weight percent, and trace elements are in ppm.

accuracy of the measured trace element concentrations is within 10%. The mineral assemblage and petrographic descriptions of the studied samples are summarized in Table 1.

[12] Polished thin sections of samples were examined in both reflected and transmitted light to identify Fe-Ti oxides and iron sulfide minerals. Selected opaque minerals were analyzed using Jeol JXA-8100 (a beam current of 10 nA at 15 kV) and Jeol JCXA-733 (a beam current of 20 nA at 15 kV) electron microprobes at Peking University and China University of Geosciences, respectively. The resolution of electron beams is about 1 μm for both. All together, 53 mineral standards, which were provided by SPI Company USA, were used to calibrate the microprobe for quantitative EMP analyses (e.g., natural hematite for Fe, and O, rutile for Ti, SiO_2 for Si, Al_2O_3 for Al, and MgO for Mg, etc.) (Table 2). Standardless analysis of iron sulfide in samples DMP-66, DMP-68 and DMP-71 was performed using a Jeol JSM-35CF SEM equipped with an energy dispersive spectrometer (EDS) and backscatter detector. The EDS spectra were collected at a beam current of 8.5 nA at 20 kV using a working distance of 11.5 mm. The concentrations of major elements in opaque grains from the three samples were calculated by neglecting insignificant elements and scaling the totals to 100% (Table 3).

[13] To determine the magnetic carriers in the samples, we used thermal demagnetization of low-temperature saturation isothermal remanent magnetization (SIRM) and high-temperature thermomagnetic (both low-field magnetic susceptibility and high-field saturation magnetization) analyses. The low-temperature experiments are sensitive to the presence of magnetite, which shows a sudden decrease of SIRM at about 120–122 K [*Verwey et al.*, 1947]. The high-temperature experiments are used to estimate the Curie temperature of magnetic minerals and assess possible mineral transformations.

[14] Low-field magnetic susceptibility analyses (heating to 700°C and cooling) were done in an argon environment using a Kappa bridge equipped with a furnace. High-field thermomagnetic analyses (J-T, heating to 700°C and cooling) were measured using a Magnetic Measurements Variable Field Translation Balance (VFTB) in a steady field of 300 mT in an argon atmosphere. For the same sample, a hysteresis loop is also measured using the VFTB with the maximum applied field of 1 T. The high-field slope of the hysteresis loop fitted to

Table 3. Representative Element Concentration Analyses for Opaque Minerals From Mafic Granulite Xenoliths Determined From Energy Dispersive Spectrometer Spectra[a]

		S		Fe		Ni		O		Mg		Ti		Al		
Sample	Count	Wt%	At%	Wt%	At%	Wt%	At%	Wt%	At%	Wt%	At%	Wt%	At%	Wt%	At%	Note[b]
DMP66	1	41.16	54.97	56.42	43.26	2.42	1.77									Pyrrhotite ($Fe_{0.79}S$)
	2	38.49	52.18	59.93	46.65	1.58	2.17									Pyrrhotite ($Fe_{0.89}S$)
	3	44.87	58.67	53.53	40.19	1.6	1.14									Pyrrhotite ($Fe_{0.69}S$)
	4			65.54	39.13			25.67	53.50	1.84	2.53	6.94	4.83			Low-Ti Titanomangtite
	5	41.09	54.90	56.58	43.40	2.33	1.70									Pyrrhotite ($Fe_{0.79}S$)
DMP68	1							34.64	61.34			65.36	38.66			Rutile (TiO_2)
	2			26.85	14.06			30.36	55.49	7.31	8.80	35.47	21.65			Mg-rich ilmenite
	3	40.11	53.94	55.40	42.77	4.49	3.30									Pyrrhotite ($Fe_{0.79}S$)
	4			31.35	16.83			29.75	55.74	4.88	6.02	33.76	21.13	0.26	0.28	Mg-rich ilmenite
	5	40.17	54.01	54.40	42.00	5.43	3.99									Pyrrhotite ($Fe_{0.78}S$)
	6			23.08	11.79			31.30	55.83	9.01	10.58	36.60	21.80			Mg-rich ilmenite
	7	42.00	55.78	58.00	44.22											Pyrrhotite ($Fe_{0.78}S$)
	8			28.31	15.22			28.66	53.79	6.61	8.17	36.41	22.82			Mg-rich ilmenite
DMP71	1			37.33	20.78			28.01	54.43	3.64	4.65	31.03	20.14			Fe, Ti oxides
	2			59.78	35.35			25.12	51.86	2.33	3.16	11.23	7.74	1.55	1.89	Mg-rich ilmenite
	3	42.50	56.28	57.50	43.72											Pyrrhotite ($Fe_{0.78}S$)
	4			35.95	19.73			28.81	55.20	4.06	5.11	31.18	19.96			Fe, Ti oxides

[a] Wt% and At% indicate weight and atom percentage, respectively.
[b] The chemical formula for iron sulfide is approximated by ignoring ions other than Fe and S.

data between 0.6 to 1 T represents the paramagnetic contribution (χ_{para}), which was subtracted from the J-T curve to isolate the signal carried by ferrimagnetic minerals. Low-temperature thermal demagnetization of an SIRM acquired at 20 K in 2.5 T (LT-SIRM) was performed with a Quantum Design Susceptometer with a temperature uncertainty of ±0.5 K. Frequency-dependent susceptibility was measured with a LakeShore Cryotronics AC Susceptometer between 40 and 4000 Hz at room temperature. Room temperature SIRM was imparted in a field of 1.5 T. Room-T remanences were measured using a 2 G cryogenic magnetometer. To further characterize the magnetic carrier of the room-T SIRM, stepwise thermal demagnetization of SIRM was performed with a temperature step of 20–30°C, with the treatment temperature denoted as T_{tr}.

4. Results

4.1. Magnetic and Geochemical Results and Bulk Properties

[15] Samples examined in this study are all mafic granulites. Magnetic susceptibilities of the mafic granulites range between 2.548 and 9.333×10^{-7} m^3 kg^{-1} with an average of 5.869×10^{-7} m^3 kg^{-1}. SIRM is between 4.81 and 85.49×10^{-4} Am^2 kg^{-1} with an average of 31.53×10^{-4} Am^2 kg^{-1} (Table 2). The relatively high MgO contents (~13.7–18.4%) of the mafic granulites and the geochemical features (e.g., positive correlations between Cr, Ni and $Mg^{\#}$)

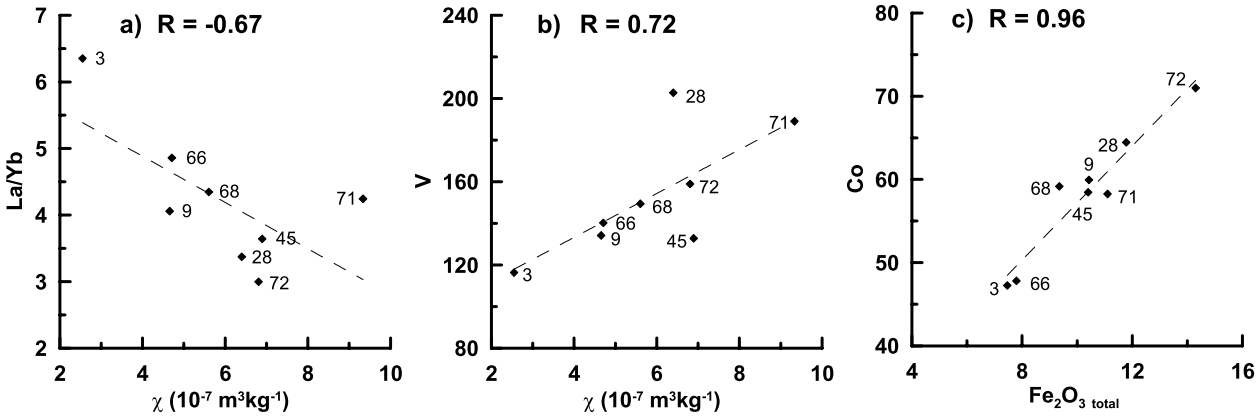

Figure 2. Major element, trace element, and susceptibility variations. (a) La/Yb versus χ. (b) V content versus χ. (c) FeO_{total} versus Co. Major oxides are reported in weight percent and trace elements in ppm. R, correlation coefficient. Numbers indicate the sample name.

can be explained and modeled by pyroxene-dominated fractional crystallization in a basaltic magma chamber [*Liu et al.*, 2001].

[16] The relationships between magnetic susceptibility and those trace elements (or element ratio) are shown in Figures 2a and 2b. Results show that in some extent, χ correlates negatively with high incompatible element ratio (e.g., La/Ya) and positively with the element V (correlation coefficients R = −0.67 and 0.72, respectively) (Figures 2a and 2b). Figure 2c shows the strong correlation between Co and FeO_{total} (R = 0.96).

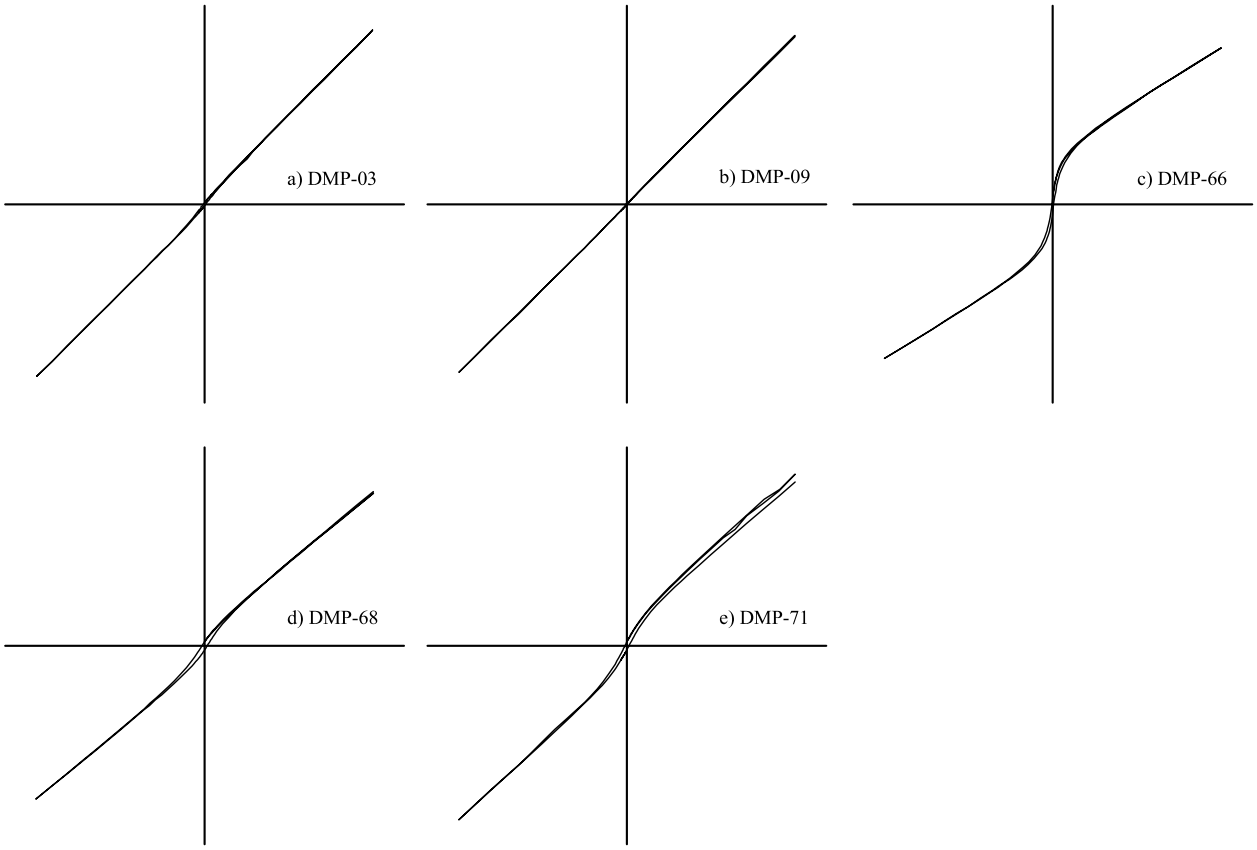

Figure 3. Hysteresis loops for representative samples.

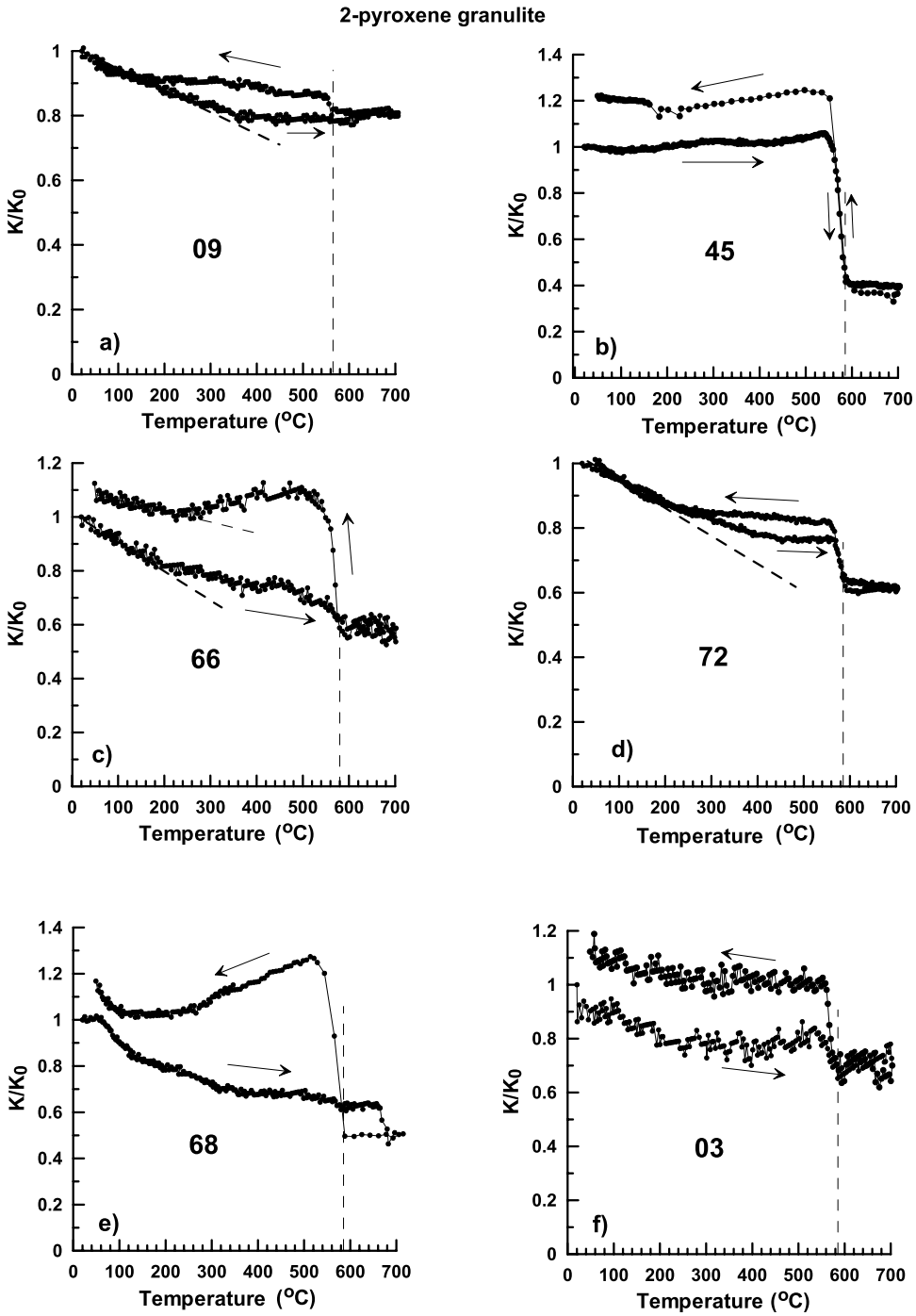

Figure 4. Temperature-dependent normalized susceptibility for selected DMP samples. Arrows represent the heating/cooling process. The gradual decrease of susceptibility is caused by paramagnetic components. Numbers indicate the sample name.

[17] The magnetic hysteresis loops for representative samples all contain a paramagnetic component (Figure 3). However, the characteristic ferrimagnetic behavior in some samples (DMP-66, DMP-68 and DMP-71 in Figure 3) was also observed.

4.2. High-Temperature-Dependent Magnetic Properties

[18] Select temperature-dependent susceptibility curves (DMP-03, 09, 45, 66, 68, and 72) are presented in Figure 4. Between room temperature

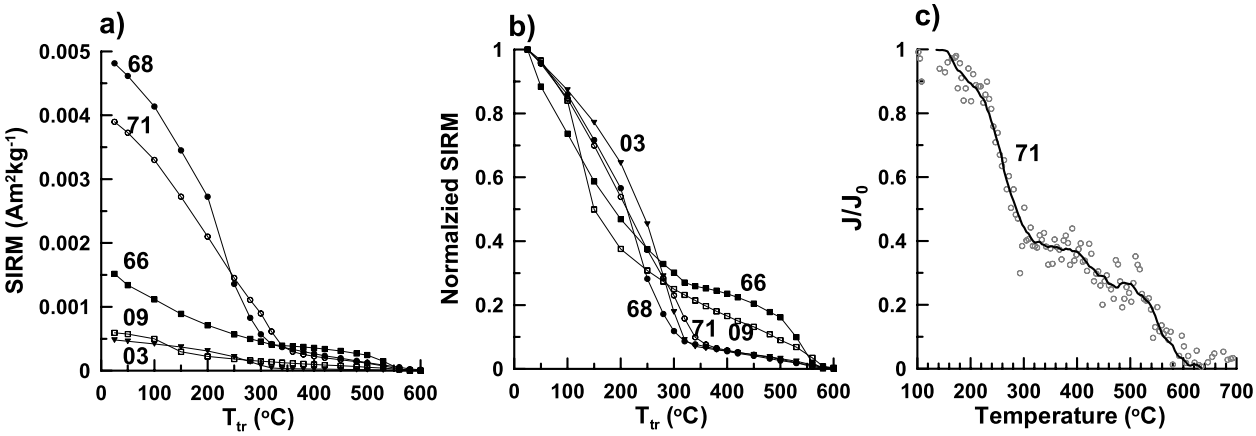

Figure 5. Stepwise thermal demagnetization spectra of SIRM. (a) Absolute and (b) normalized values. (c) The normalized temperature dependence of magnetization curve for sample DMP71. The open circles are the corrected data, and the thin curve indicates the 7-point smoothing trend.

and ~350°C, the gradual decrease of susceptibility is considered due to paramagnetic components. The cooling curves for all samples are higher than the heating curves. The ~580°C Curie temperatures of the cooling curves indicates that the newly formed magnetic mineral is magnetite for most samples. The relative reversible features for samples DMP-45 and 72 indicate that magnetite is a dominant magnetic phase in the fresh samples (Figures 4b and 4d). Samples DMP-66 and 68 have an initial Curie temperature of about 680°C, indicating the presence of hematite, but the cooling curve indicates a mineral transformation from hematite to magnetite (Figures 4c and 4e). Samples DMP-09 and DMP-03 appeared very weakly magnetic, but show a small transition near 580°C for both heating and cooling (Figures 4a and 4f).

[19] The unblocking temperature can be used to identify some magnetic minerals in mafic granulite xenoliths. The stepwise thermal demagnetization of SIRM for samples DMP-03, 09, 66, 68 and 71 are shown in Figures 5a and 5b. For samples DMP-68 and 71 about 90% of their room-T SIRM has been demagnetized by 350°C. A small fraction (~10%) of the SIRM was further demagnetized at about 580°C, which corresponds to magnetite. Samples DMP-09 and 66 have smaller room-T SIRM values, and the relative contribution of magnetite to the room-T SIRM for these two samples is higher than that of the others (Figure 5b). The sample DMP-03 has a thermal demagnetization spectrum similar to those of samples DMP-68 and 71 (Figure 5b). The normalized temperature dependence of magnetization curve for sample DMP-71 after paramagnetic correction using the software Rockmag Analyzer

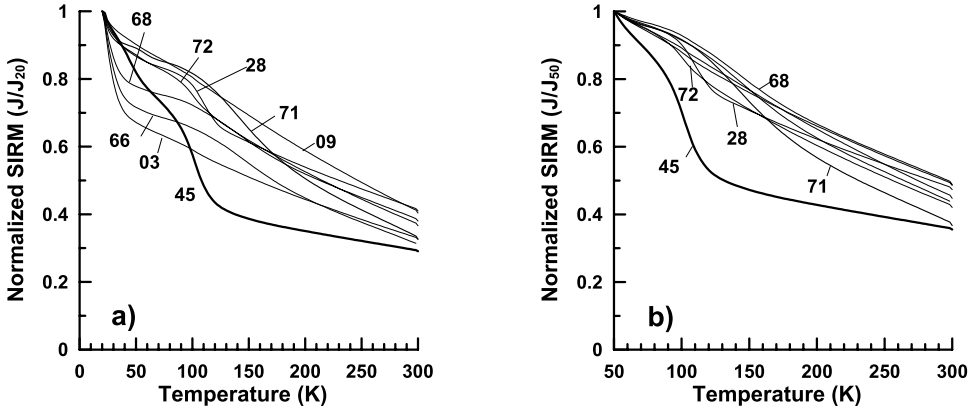

Figure 6. Low-temperature thermal demagnetization of 20K SIRM, normalized to remanences at (a) 20 K and (b) 50 K. Numbers indicate the sample name.

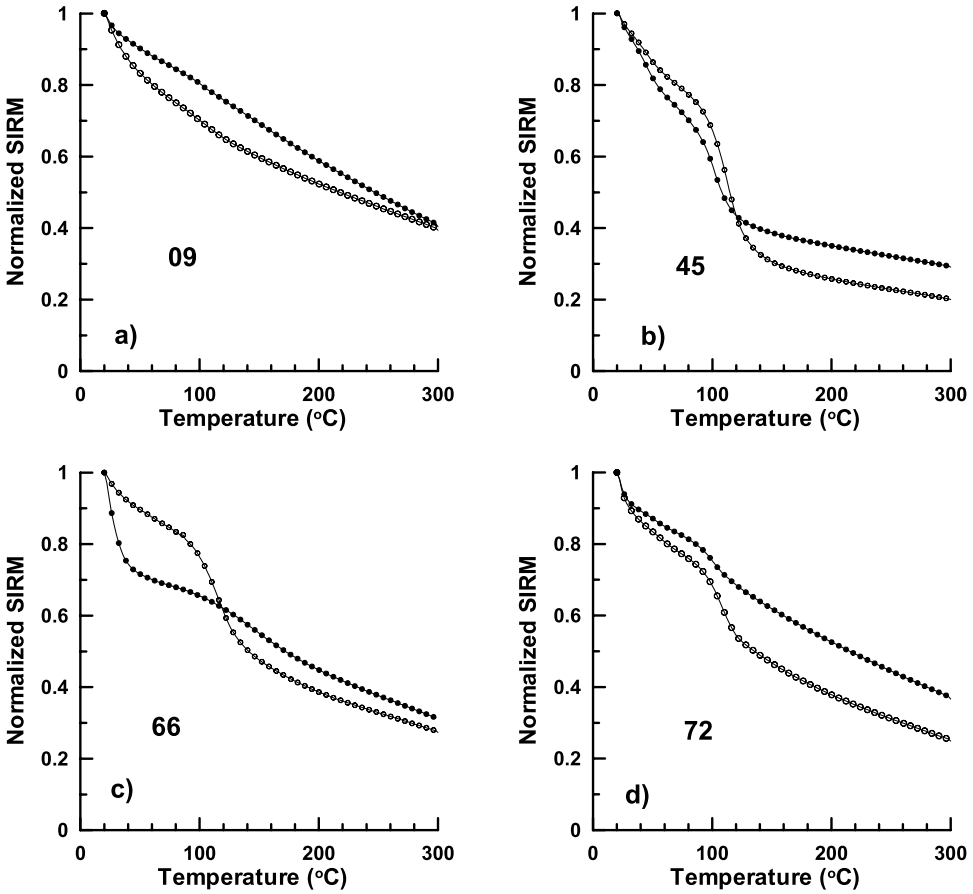

Figure 7. Comparison of room temperature SIRM thermal demagnetization before (solid circles) and after (open circles) heating samples to 700°C.

Version 1.0 released by Roman Leonhardt [*Leonhardt*, 2006] is shown in Figure 5c. The two Curie temperatures of about 320°C and 580°C for the heating curve correspond to pyrrhotite [*Dekkers*, 1989] and magnetite, respectively.

4.3. Low-Temperature Magnetic Properties

[20] Normalized LT-SIRM curves are shown in Figure 6. Sample DMP-45 exhibits an apparent Verwey transition around 120 K, indicating the existence of magnetite. Samples DMP-03, 66, and 68 show sudden drops in remanences around 30 K, but no Verwey transitions was observed, whereas, samples DMP-72 and 28 show both weak Verwey and 30 K transitions (Figure 6a). To avoid the effects of the ~30 K transition, Figure 6b shows the LT-SIRM curves normalized by the remanence at 50 K. Clearly, sample DMP-45 has a distinctly different low-temperature behavior compared to the others. Comparison of LT-SIRM curves of raw material and the samples heated to 700°C are shown in Figure 7. For samples DMP-45, 66, and 72, the thermal products have an enhanced Verwey transition.

4.4. Frequency Dependencies of Susceptibility

[21] Figure 8 illustrates the frequency dependencies of susceptibility. Previous studies have shown that the susceptibility of superparamagnetic (SP) grains is negatively correlated with the measured frequency, and the frequency dependence of susceptibility has been widely used to quantify the contributions of such extremely fine-grained particles [*Stephenson*, 1971; *Dearing et al.*, 1996]. Figure 8 shows that the susceptibilities of all samples are independent of frequency, indicating that the remanence decay with increasing temperatures is not caused by SP grains.

4.5. Backscattering Electron Images and Types of Opaque Minerals

[22] The backscatter electron images of the opaque minerals in four samples are shown in Figure 9.

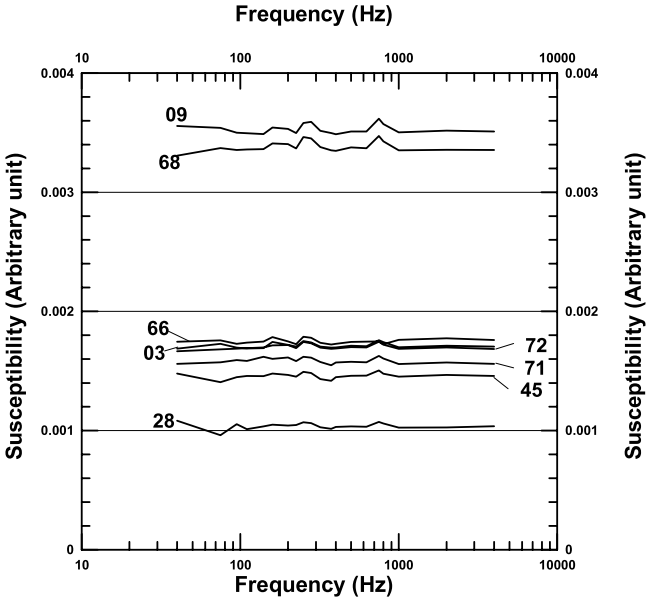

Figure 8. Frequency-dependent susceptibility for mafic granulite xenoliths. Numbers indicate the sample name.

The coarse-grained opaque mineralogy consists mainly of Mg-rich ilmenite, pyrrhotite and minor titanomagnetite with different grain sizes and concentrations among samples. For DMP-28 and 66 (Figures 9a and 9c), the opaque minerals are hosted by clinopyroxene and plagioclase. But for DMP-68 (Figure 9b), it seems that the opaque minerals are located at grain boundaries of clinopyroxene and plagioclase. Sample DMP-71 (Figure 9d) is dominated solely by clinopyroxene, but the

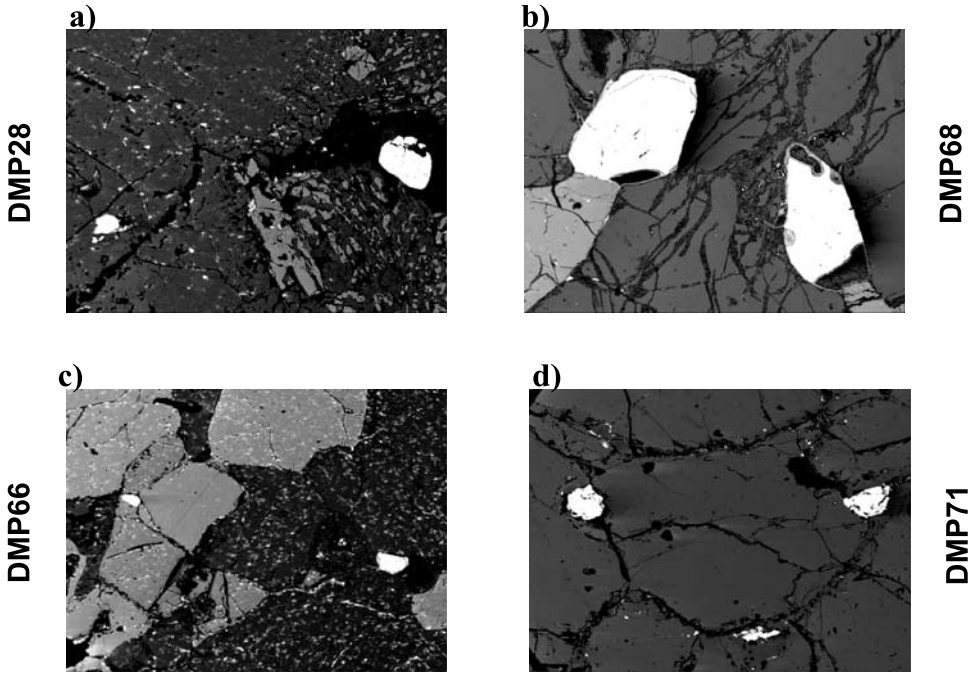

Figure 9. Backscatter images of (a) DMP28 (light gray is Cpx; dark gray is Pl), (b) DMP68 (light gray is Cpx; dark gray is Pl, (c) DMP66 (light gray is Cpx; dark gray is Pl), and (d) DMP71 (gray is Cpx). Field of view: 927 μm wide in Figures 9a, 9b, and 9d and 1854 μm wide in Figure 9c. Cpx and Pl represent clinopyroxene and plagioclase, respectively. White minerals are Mg-rich ilmenites. Numbers indicate the sample name.

Table 4. Representative Oxide Analyses for Opaque Minerals From Mafic Granulite Xenoliths (wt.%)

Number	Count	SiO_2	TiO_2	Al_2O_3	FeO	MnO	MgO	CaO	Na_2O	K_2O	Cr_2O_3	Total	Chemical Formula[a]
03	1	0.163	58.714	0.000	31.378	0.241	11.174	0.032	0.000	0	0.300	102.002	$(Fe_{0.59}Mg_{0.38})TiO_3$
	2	0.000	57.278	0.000	31.251	0.402	10.728	0.004	0.000	0	0.210	99.873	$(Fe_{0.61}Mg_{0.37})TiO_3$
	3	0.000	58.048	0.106	30.050	0.240	10.943	0.009	0.000	0	0.219	99.615	$(Fe_{0.58}Mg_{0.38})TiO_3$
	4	0.240	54.986	0.280	33.589	0.242	8.537	0.112	0.000	0	0.185	98.171	$(Fe_{0.67}Mg_{0.31})TiO_3$
09	1	0	54.945	0.312	34.617	0.315	8.475	0	0	0	0.238	98.902	$(Fe_{0.69}Mg_{0.30})TiO_3$
	2	0	55.687	0	34.240	0.347	8.253	0	0	0	0.701	99.228	$(Fe_{0.68}Mg_{0.30})TiO_3$
45	1	0	56.005	0	33.670	0.132	7.385	0.006	0	0	0.157	97.355	$(Fe_{0.68}Mg_{0.27})TiO_3$
	2	0	53.413	0	36.683	0.187	6.619	0.023	0	0	0.226	97.151	$(Fe_{0.76}Mg_{0.25})TiO_3$
	3	0	57.756	0	34.237	0.152	8.196	0.001	0.244	0	0.120	100.706	$(Fe_{0.67}Mg_{0.29})TiO_3$
	4	0	56.143	0	35.821	0.139	7.715	0.052	0.045	0	0.133	100.048	$(Fe_{0.71}Mg_{0.28})TiO_3$
	5	0.040	54.620	0	38.680	0.320	6.03	0.00	0.04	0	0.130	99.860	$(Fe_{0.78}Mg_{0.22})TiO_3$
	6	0.030	55.630	0	38.660	0.380	5.98	0.00	0.08	0	0.100	100.860	$(Fe_{0.71}Mg_{0.21})TiO_3$
66	1	0	54.250	0.363	36.121	0.244	8.617	0.033	0	0	0.262	99.890	$(Fe_{0.72}Mg_{0.31})TiO_3$
	2	0	0	0	73.931	0.010	0	0.049	0	0	0.109	74.099	Fe-sulfide
68	1	0	0	0	75.104	0	0	0.040	0.291	0	0	75.435	Fe-sulfide
	2	0	0	0	74.147	0	0.022	0.007	0	0	0	74.176	Fe-sulfide
	3	0	55.268	0	38.883	0.366	4.919	0.025	0.060	0	0.478	99.999	$(Fe_{0.79}Mg_{0.18})TiO_3$
	4	0	55.246	0	38.960	0.257	4.929	0	0	0	0.513	99.905	$(Fe_{0.79}Mg_{0.18})TiO_3$
	5	0	0	0	74.972	0	0	0.004	0	0	0.073	75.049	Fe-sulfide
71	1	0	0	0	73.943	0	0	0	0	0	0	73.943	Fe-sulfide
	2	0	50.863	0.226	40.338	0.319	6.229	0.010	0	0	0.213	98.198	$(Fe_{0.84}Mg_{0.23})TiO_3$
	3	0	51.258	0.155	39.983	0.239	6.405	0	0	0	0.294	98.334	$(Fe_{0.83}Mg_{0.24})TiO_3$
72	1	0	56.724	0.000	35.324	0.1444	7.667	0.000	0	0	0.141	100.000	$(Fe_{0.70}Mg_{0.27})TiO_3$
	2	0	57.040	0.107	33.279	0.260	9.255	0.051	0	0	0.007	99.999	$(Fe_{0.65}Mg_{0.33})TiO_3$
	3	0	55.731	0.100	32.250	0.161	9.059	0.000	0	0	0.159	97.460	$(Fe_{0.65}Mg_{0.33})TiO_3$
	4	0	56.609	0.000	33.202	0.156	7.415	0.011	0	0	0.243	97.636	$(Fe_{0.67}Mg_{0.27})TiO_3$

[a] The chemical formulas are approximated by ignoring cations other than Fe, Ti, and Mg.

opaque minerals are located in fractures within clinopyroxene.

[23] Electron microprobe (EMP) analysis of opaque minerals in polished thin sections reveal the existence of Mg-rich ilmenite and Fe-sulfides (Table 4). The total TiO_2 contents of Mg-rich ilmenite particles are >50 wt%. The FeO and MgO vary significantly among different samples, between ~30 wt% and ~40 wt%, and between ~6 wt% and ~11 wt%, respectively. The Fe-sulfide minerals are mainly in samples DMP-66, 68 and 71 with FeO contents ranging from 73.931% to 75.104% (Table 4).

[24] The energy-dispersive analysis results for samples DMP-66, 68 and 71 are shown in Table 3. For pyrrhotite particles, the Fe/S atom ratio is about 0.8, which corresponds to $Fe_{0.8}S$. This Fe/S ratio is lower than that (~0.9) of the antiferromagnetic phases (e.g., Fe_9S_{10}, $Fe_{11}S_{12}$), and even lower than that (0.875) of ferromagnetic phase (Fe_7S_8). Nevertheless, the electron microprobe and energy-dispersive spectrometry analyses unambiguously indicate the presence of iron sulfide with the S content higher than that of pure pyrite. Pyrrhotite and Fe-Ti oxides (e.g., low-Ti titanomagnetite) appear to be the dominant ferromagnetic minerals (Table 3).

5. Discussion

5.1. Opaque Mineralogy of Mafic Granulite Xenoliths

[25] The dominant opaque mineral in our studied samples is Mg-rich ilmenite (Table 4). It is confirmed by both of paramagnetic component in magnetic hysteresis loops (Figure 3) and the gradual decreasing of susceptibility from room temperature to 350°C in Figure 4. The high-temperature susceptibility curves reveal that samples DMP-45 and 72 contain magnetite (Figures 4b and 4d). The low-temperature results also indicate that samples DMP-28, 45, and 72 have detectable Verwey transitions, which indicate the presence of magnetite (Figure 6). This is consistent with the T_c and T_b of magnetite from the high-temperature thermomagnetic analysis (Figures 4 and 5). In addition, the about 300°C T_b and T_c (Figure 5) as well as the SEM and EMP analyses indicate that DMP-66, DMP-68 and DMP-71 contain pyrrhotite (Table 3 and Table 4). This can be further confirmed by the

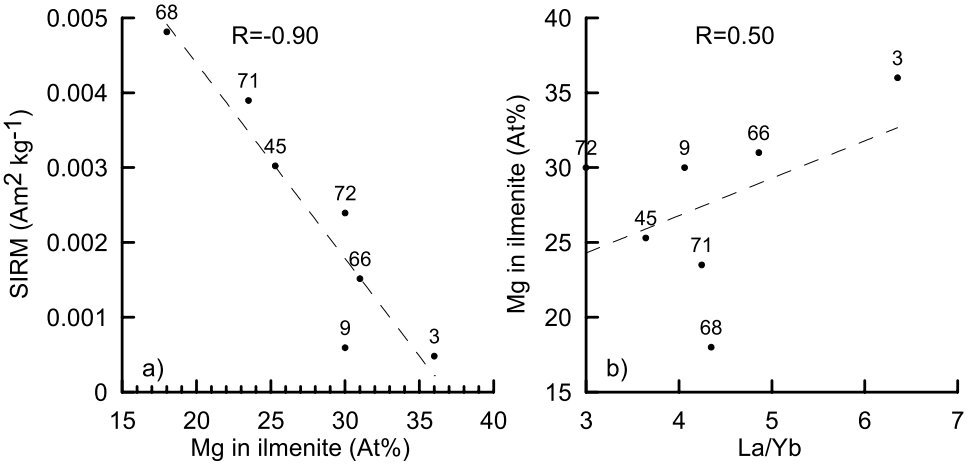

Figure 10. Correlations (a) between SIRM and the Mg content in ilmenite crystals and (b) between the Mg content in ilmenite crystals and La/Yb. Numbers indicate the sample name.

sharp remanence drops in these samples near 30 K (Figure 6a), which is associated with the pyrrhotite low-T transition [e.g., *Dekkers et al.*, 1989; *Rochette et al.*, 1990]. Therefore, the dominant ferromagnetic phases in our studied samples are pyrrhotite and magnetite with different contributions in different samples (Figure 5).

[26] The average magnetic susceptibility of pure magnetite is about 4 times that of pyrrhotite [*Carmichael*, 1982], therefore, even though the concentration of magnetite is low relative to the concentration of pyrrhotite, the magnetite signal can overwhelm the contribution from pyrrhotite in thermomagnetic curves and this is probably main reason for the absence of a pyrrhotite T_c in high-temperature susceptibility-dependent temperature curves (Figure 4). The inconsistency between rock magnetic and mineralogy for magnetite for a few samples could be attributed mainly to very low concentration of magnetite, which cannot be detected by EMP and SEM analyses, but by sensitive rock magnetic methods [*Dunlop and Özdemir*, 1997].

5.2. Relationship Between Magnetic Properties and Fractional Crystallization for Mafic Granulite Xenoliths

[27] The fractional crystallization of mafic granulite xenoliths and terrance (this occurs in igneous rock or in metamorphic granulites) is an important geological process in the continental lower crust [*Schlinger*, 1985]. DMP xenoliths were formed by fractional crystallization on the basis of the following petrological and geochemical information [*Liu et al.*, 2001]: (1) the continuous thick layers of alternating plagioclase and pyroxene in several xenoliths point to their origin as products of accumulation in a magma chamber; (2) REE patterns of pyroxenites and some two-pyroxene granulites and garnet-bearing mafic granulites are typical of clinopyroxene-rich cumulates derived from LREE-enriched magmas; (3) the positive correlations between Cr, Ni and $Mg^{\#}$ for most DMP-xenoliths suggest that they are products of the fractional crystallization of olivine, pyroxene and plagioclase; (4) the high Al_2O_3 contents and positive Eu anomalies of some xenoliths suggesting plagioclase-dominated cumulates. Although Sr, La and Yb are all incompatible elements during pyroxene-dominated crystallization, La is more incompatible than Yb. Thus, the Sr contents and the La/Yb ratios of cumulates will increase with fractional crystallization, and they can be used as proxies for the degree of fractional crystallization. For example, from the consideration of the La/Yb ratio, samples DMP-68 and 71 have undergone a lower degree of fractional crystallization than samples DMP-03, 09 and 66 (Figure 10a).

[28] The negative correlations between χ and the La/Ya ratio (correlation coefficient = −0.67) suggest that χ decreases with increasing the degree of fractional crystallization (Figure 2b). V and Co are weakly compatible in clinopyroxene (Kd(V) = 1.81 [*Jenner et al.*, 1994] and Kd(Co) = 1.02 [*Villemant et al.*, 1981]), and highly incompatible in plagioclase [*Bougault and Hekinian*, 1974; *Paster et al.*, 1974]. Therefore, the bulk partition coefficients of V and Co are <1 (assuming accumulates composed of 60% cpx + 40pl) if no minor minerals (e.g., Ti-Fe oxide) enriched in V and Co crystallized. The

correlations between Co and FeO_{total} implies that Co is controlled by Ti-Fe-oxides rather than silicate minerals (e.g., cpx). On the other hand, χ correlates well with V (Figure 2). A linear correlation is observed between SIRM and Mg content in the Mg-rich ilmenite (Figure 10a). Moreover, the Mg content in the Mg-rich ilmenite is positively correlated with the La/Yb ratio (Figure 10b), which increases with increasing degree of fractional crystallization [*Liu et al.*, 2001]. This indicates that the Mg content in ilmenite may be controlled by the fractional crystallization. The decreases in SIRM with increasing the degree of the fractional crystallization could be due to the gradual consumption of pyrrhotite (Figure 5a). But the exact relationship between magnetic mineralogy and fractional crystallization and the consequences for the distribution on magnetism in the lower crust deserves more detailed study.

6. Conclusions

[29] The integrated magnetic, geochemical and mineralogical analyses suggest that the major opaque mineral in the mafic granulite xenoliths from the Damaping (DMP), Hannuoba region, North China Craton is paramagnetic Mg-rich ilmenite. Pyrrhotite, hematite and magnetite are present in samples but their concentrations vary greatly among samples, which may account for the wide range of magnetic properties. Our results show that the opaque minerals in these samples reflect the geochemical partitioning associated with the fractional crystallization process. As is the Mg content in ilmenite may be also controlled by the fractional crystallization. The relationship between rock magnetism and fractional crystallization appears real, but more research is required to relate these processes to the distribution of magnetism in the lower crust.

Acknowledgments

[30] This paper was supported by the Major State Basic Research Development Program of China ("973 Project" 2003CB716506), the National Natural Science Foundation of China (NSFC grants 40474025, 40473013, and 40521001), and the Program for Changjiang Scholars and Innovative Research Team in University (IRT0441). Qingsong Liu is supported by the "100 Talent program of the Chinese Academy of Sciences." Low-temperature experiments were conducted at the Institute for Rock Magnetism (IRM), which is supported by the W.M. Keck Foundation, the Earth Science Division of the U.S. National Science Foundation, and the University of Minnesota. D. J. Dunlop provided helpful comments for a previous version of the manuscript. We further thank an anonymous reviewer and Michael Jackson (the associate editor) for their instructive comments, which significantly improved the quality of this study.

References

Arkani-Hamed, J., and J. Dyment (1996), Magnetic potential and magnetization contrasts of Earth's lithosphere, *J. Geophys. Res.*, *101*, 11,401–11,425.

Arkani-Hamed, J., and D. W. M. Strangway (1985), Lateral variations of apparent magnetic susceptibility of lithosphere deduced from Magsat data, *J. Geophys. Res.*, *90*, 2655–2664.

Belluso, E., G. Biino, and R. Lanza (1990), New data on the rock magnetism in the Ivrea-Verbano Zone (northern Italy) and its relations to the magnetic anomaly, *Tectonophysics*, *182*, 79–89.

Bougault, H., and R. Hekinian (1974), Rift Valley in the Atlantic Ocean near 36°50′ N: Petrology and geochemistry of basaltic rocks, *Earth Planet. Sci. Lett.*, *24*, 249–261.

Carmichael, R. S., (Ed.) (1982), *Handbook of Physical Properties of Rocks*, vol. II, 268 pp., CRC Press, Boca Raton, Fla.

Chen, S. H., S. Y. O'Reilly, X. Zhou, W. L. Griffin, G. Zhang, M. Sun, J. Feng, and M. Zhang (2001), Thermal and petrological structure of the lithosphere beneath Hannuoba, Sino-Korean Craton, China: Evidence from xenoliths, *Lithos*, *56*, 267–301.

Dearing, J. A., R. J. L. Dann, K. Hay, J. A. Lees, P. J. Loveland, B. M. Maher, and K. O'Grady (1996), Frequency-dependent susceptibility measurements of environmental materials, *Geophys. J. Int.*, *124*, 228–240.

Dekkers, M. J. (1989), Magnetic properties of natural pyrrhotite. II. High and low temperature behaviors of Jrs and TRM as a function of grain size, *Phys. Earth Planet. Inter.*, *57*, 266–283.

Dekkers, M. J., J. L. Mattéi, G. Fillion, and P. Rochette (1989), Grain-size dependence of the magnetic behavior of pyrrhotite during its low-temperature transition at 34 K, *Geophys. Res. Lett.*, *16*, 855–858.

Downes, H. (1993), The nature of the lower continental crust of Europe: Petrological and geochemical evidence from xenoliths, *Phys. Earth Planet. Inter.*, *79*, 195–218.

Dunlop, D. J., and Ö. Özdemir (1997), *Rock Magnetism: Fundamentals and Frontiers*, pp. 288–390, Cambridge Univ. Press, New York.

Fan, Q. C., R. X. Liu, H. M. Li, N. Li, J. L. Sui, and Z. R. Lin (1998), Zircon geochronology and rare earth element geochemistry of granulite xenoliths from Hannuoba (in Chinese), *Chin. Sci. Bull.*, *43*, 133–137.

Haggerty, S. E., and P. B. Toft (1985), Native iron in the continental lower crust: Petrological and geophysical implications, *Science*, *229*, 647–649.

Hemant, K., and S. Maus (2005), Geological modeling of the new CHAMP magnetic anomaly maps using a geographical information system technique, *J. Geophys. Res.*, *110*, B12103, doi:10.1029/2005JB003837.

Jenner, G. A., S. F. Foley, S. E. Jackson, T. H. Green, B. J. Fryer, and H. P. Longerich (1994), Determination of partition coefficients for trace elements in high pressure-temperature experimental run products by laser ablation microprobe-inductively coupled plasma-mass spectrometry (LAM-ICP-MS), *Geochim. Cosmochim. Acta*, *58*, 5099–5103.

Kasama, T., S. A. McEnroe, N. Ozaki, T. Kogure, and A. Putnis (2004), Effects of nanoscale exsolution in hematite-ilmenite

on the acquisition of stable natural remanent magnetization, *Earth Planet. Sci. Lett.*, *224*, 461–475.

Kay, R. W., and S. M. Kay (1981), The nature of lower continental crust: Inferences from geophysics, surface geology and crustal xenoliths, *Rev. Geophys.*, *19*, 271–297.

Kelso, P. R., S. K. Baberjii, and C. Teyssier (1993), Rock magnetic properties of the Arunta Block, central Australia, and their implication for the interpretation of long-wavelength magnetic anomalies, *J. Geophys. Res.*, *98*, 15,987–15,999.

Kletetschka, G., and P. J. Wasilewski (2002), Grain size limit for SD hematite, *Phys. Earth Planet. Inter.*, *129*, 173–179.

Leonhardt, R. (2006), Analyzing rock magnetic measurements: The RockMagAnalyzer 1.0 software, *Comput. Geosci.*, *32*, 1420–1431.

Liu, Q. S., and S. Gao (1992), Geophysical properties of the lower crustal granulites from the Qinling orogenic belt, China, *Tectonophysics*, *204*, 401–408.

Liu, Q. S., and F. X. Lu (1992), Magnetic petrology of ultramafic xenoliths from Dalongwan, Huinan, Jilin Province, China, *Chin. Sci. Bull.*, *7*, 582–586.

Liu, Q. S., S. Gao, and Y. S. Liu (2000), Magnetic structure of the continental crustal cross-section in central North China Craton, *J. Geodyn.*, *29*, 1–13.

Liu, Q. S., Q. S. Liu, Z. M. Zhang, T. Yang, and Y. Y. Fu (2004), Serpentinized peridotite as the source of the aeromagnetic anomalies, *J. China Univ. Geosci.*, *15*, 416–419.

Liu, Q. S., Q. S. Liu, Z. M. Zhang, H. J. Xu, L. S. Chan, T. Yang, and Z. M. Jin (2007), Magnetic properties of ultrahigh-pressure eclogites controlled by retrograde metamorphism: A case study from the ZK703 drillhole in Donghai, eastern China, *Phys. Earth Planet. Inter.*, *160*, 181–191.

Liu, Y. S., S. Gao, S. Y. Jin, S. H. Hu, J. L. Feng, Z. B. Zhao, and M. Sun (2001), Geochemistry and petrogenesis of lower crustal xenoliths from Hannuoba, North China: Implications for the continental lower crustal composition and evolution at convergent margin, *Geochim. Cosmochim. Acta*, *65*, 2589–2604.

Liu, Y. S., S. Gao, X. M. Liu, X. M. Chen, W. L. Zhang, and X. C. Wang (2003), Thermodynamic evolution of lithosphere of the North China Craton: Records from lower crust and upper mantle xenoliths from Hannuoba, *Chin. Sci. Bull.*, *48*, 2371–2377.

Liu, Y. S., S. Gao, H. L. Yuan, L. Zhou, X. M. Liu, X. C. Wang, Z. C. Hu, and L. S. Wang (2004), U-Pb zircon dates and Nd, Sr and Pb isotopes of lower crustal xenoliths from North China Craton: Insights on evolution of lower continental crust, *Chem. Geol.*, *21*, 87–109.

McEnroe, S. A., P. Robinson, and P. T. Panish (2001), Aeromagnetic anomalies, magnetic petrology, and rock magnetism of hemo-ilmenite- and magnetite-rich cumulate rocks from the Sokndal Region, South Rogaland, Norway, *Am. Mineral.*, *86*, 1447–1468.

McEnroe, S. A., F. Langenhorst, P. Robinson, G. D. Bromiley, and C. S. J. Shaw (2004), What is magnetic in the lower crust?, *Earth Planet. Sci. Lett.*, *226*, 175–192.

Paster, T. P., D. S. Schauwecker, and L. A. Haskin (1974), The behavior of some trace elements during solidification of the Skaergaard layered series, *Geochim. Cosmochim. Acta*, *38*, 1549–1577.

Pechersky, D. M., and Y. S. Genshaft (2002), Petromagnetism of the continental crust: A summary of 20th century research, Izv. Russ, *Acad. Sci. Phys. Solid Earth, Engl. Transl.*, *38*, 4–36.

Pikington, M., and J. A. Percival (1999), Crustal magnetization and long-wavelength aeromagnetic anomalies of the Minto Block, Quebec, *J. Geophys. Res.*, *104*, 7513–7526.

Pikington, M., and J. A. Percival (2001), Relating crustal magnetization and satellite-altitude magnetic anomalies in the Ungava peninsula, northern Quebec, Canada, *Earth Planet. Sci. Lett.*, *194*, 127–133.

Ramachandran, C. (1990), Metamorphism and magnetic susceptibilities in south Indian granulite terrain, *J. Geol. Soc. India*, *35*, 395–403.

Robinson, P., R. Harrison, S. A. McEnroe, and R. Hargraves (2002), Lamellar magnetism in the hematite-ilmenite series as an explanation for strong remanent magnetization, *Nature*, *418*, 517–520.

Robinson, P., R. Harrison, S. A. McEnroe, and R. Hargraves (2004), Nature and origin of lamellar magnetism in the hematite-ilmenite series, *Am. Mineral.*, *89*, 725–747.

Rochette, P., G. Fillion, J. L. Matt Mattéi, and M. J. Dekkers (1990), Magnetic transition at 30–34 Kelvin in pyrrhotite: Insight into a widespread occurrence of this mineral in rocks, *Earth Planet. Sci. Lett.*, *98*, 319–328.

Rudnick, R. L. (1992), Xenoliths-Samples of the lower continental crust, in *Continental Lower Crust*, edited by D. M. Fountain, R. Arculus, and R. W. Kay, pp. 269–316, Elsevier, New York.

Rudnick, R. L., and D. M. Fountain (1995), Nature and composition of the continental crust: A lower crustal perspective, *Rev. Geophys.*, *33*, 267–309.

Rudnick, R. L., and S. Gao (2003), Composition of the continental crust, in *The Crust: Treatise On Geochemistry*, edited by R. L. Rudnick, pp. 1–70, Elsevier, Oxford, U. K.

Schlinger, C. M. (1985), Magnetization of lower crust and interpretation of regional magnetic anomalies: Example from Lofoten and Vesterålen, Norway, *J. Geophys. Res.*, *90*, 11,484–11,504.

Schlinger, C. M., and D. R. Veblen (1989), Magnetism and transmission electron microscopy of Fe-Ti oxides and pyroxenes in a granulite from Lafaten, Norway, *J. Geophys. Res.*, *94*, 14,009–14,026.

Shive, P. N., and D. M. Fountain (1988), Magnetic mineralogy in an Archean crustal cross section: Implications for crustal magnetization, *J. Geophys. Res.*, *93*, 12,177–12,186.

Shive, P. N., R. J. Blakely, B. R. Frost, and D. M. Fountain (1992), Magnetic properties of the lower continental crust, in *Continental Lower Crust*, edited by D. M. Fountain, R. Arculus, and R. W. Kay, pp. 145–200, Elsevier, New York.

Stephenson, A. (1971), Single domain grain distribution I. A method for the determination of single domain grain distribution, *Phys. Earth Planet. Inter.*, *4*, 353–360.

Verwey, E. J., P. W. HaaYman, and F. C. Romeijn (1947), Physical properties and cation arrangement of oxides with spinal structures, *J. Chem. Phys.*, *15*, 181–189.

Villemant, B., H. Jaffrezic, J. L. Joran, and M. Treuil (1981), Distribution coefficients of major and trace elements: Fractional crystallization in the alkali basalt series of Chaine des Puys (Massif Central, France), *Geochim. Cosmochim. Acta*, *45*, 1997–2016.

Warner, R. D., and P. J. Wasilewski (1995), Magnetic petrology of lower crust and upper mantle xenoliths from McMurdo Sound, Antarctica, *Tectonophysics*, *249*, 69–92.

Warner, R. D., and P. J. Wasilewski (1997), Magnetic petrology of arc xenoliths from Japan and Aleutian Islands, *J. Geophys. Res.*, *102*, 20,225–20,243.

Wasilewski, P. J. (1987), Magnetic properties of mantle xenoliths and magnetic character of the crust-mantle boundary, in *Mantle Xenoliths*, edited by P. H. Nixon, pp. 577–588, John Wiley, Chichester, N. Y.

Wasilewski, P. J., and D. M. Fountain (1982), The Ivrea Zone as a model for the distribution of magnetization in the continental crust, *Geophys. Res. Lett.*, *9*, 333–336.

Wasilewski, P. J., and M. A. Mayhew (1982), Crustal xenoliths magnetic properties and long wavelength anomaly source requirements, *Geophys. Res. Lett.*, *9*, 329–332.

Wasilewski, P. J., and R. D. Warner (1988), Magnetic petrology of deep crustal rocks-Ivrea Zone, Italy, *Earth Planet. Sci. Lett.*, *87*, 347–361.

Wilde, S. A., X. H. Zhou, A. A. Nemchin, and M. Sun (2003), Mesozoic crust-mantle interaction beneath the North China Craton: A consequence of the dispersal of Gondwanaland and accretion of Asia, *Geology*, *31*, 817–820.

Willams, M. C., P. N. Shive, D. M. Fountain, and B. R. Frost (1985), Magnetic properties of exposed deep crustal rocks from the Superior Province of Manitoba, *Earth Planet. Sci. Lett.*, *76*, 176–184.

Zhang, J. S., and J. D. A. Piper (1994), Magnetic fabric and post-orogenic uplift and cooling magnetizations in a Precambrian granulite terrain: The Datong-Huai'an region of the North China shield, *Tectonophysics*, *234*, 227–246.

Zhao, G. C., P. A. Cawood, S. A. Wilde, M. Sun, and L. Z. Lu (2000), Metamorphism of basement rocks in the Central Zone of the North China Craton: Implications for paleoproterozoic tectonic evolution, *Precambrian Res.*, *103*, 55–88.

Zhu, B. Q. (1998), *Theory and Applications of Isotope Systematics in Geosciences: Evolution of Continental Crust and Mantle in China* (in Chinese), Science Press, Beijing.